

---

## Multi-temporal analysis of submarine sand dunes morphodynamics (Bay of Brest, Brittany, France): A marker of sediment pathways in a macrotidal environment open to sea swells

Belleney Deborah <sup>1,\*</sup>, Ehrhold Axel <sup>2</sup>, Le Dantec Nicolas <sup>3,4</sup>, Le Roy Pascal <sup>3</sup>, Jouet Gwenael <sup>2</sup>

<sup>1</sup> Institut Universitaire Européen de la Mer, Geomer - UMR 6554 CNRS LETG, 29280, Plouzané, France

<sup>2</sup> IFREMER, Géosciences Marines, Centre de Brest, 29280, Plouzané, France

<sup>3</sup> Institut Universitaire Européen de la Mer, UMR 6538 Géosciences Océan, Technopôle Brest-Iroise, 29280, Plouzané, France

<sup>4</sup> Institut Universitaire Européen de la Mer, UMS 3113, Technopôle Brest-Iroise, 29280, Plouzané, France

\* Corresponding author : Deborah Belleney, email address : [deborah.belleney@univ-brest.fr](mailto:deborah.belleney@univ-brest.fr)

---

### Abstract :

Sediment structures including submarine banks and dune fields are ubiquitous on tide-dominated continental inner shelves such as in the Iroise Sea. These are of current interest to human activities in several respects: they constitute an obstacle to navigation, they are dredged for beach nourishment or exploited for marine aggregates. In addition, the morphodynamic characterising of these sedimentary structures improves the knowledge of the sediment transfers that occur in coastal areas. This study documents a submarine sand dune field located along the northern flank of the Goulet channel connecting the Bay of Brest to the Iroise Sea and the Bay of Biscay. Subject to a macrotidal regime with strong currents, and to large waves during storm events, this sedimentary system features large dunes with very high migration rates. The analysis of six bathymetric datasets (from March 2013 to October 2019) allows specifying the morphodynamic characteristics of this small dune field about 3.5 km in length and 500 m in width. These dunes have heights on the order of 0.5 m–3.7 m with migration rates that can vary significantly within the range from 10 m/yr to 70 m/yr. The results highlight that the ebb tidal current and slope of the channel are the main factors controlling the evolution of these biogenic sandy structures migrating offshore (SW). Furthermore, seasonal variations in coastal hydrodynamics forcing, driven by tidal currents, appear to affect the temporal and spatial evolution of the dunes at this shorter time scale. This paper proposes a model of sediment transport patterns at the mouth of the bay of Brest according dune field characteristic, strong ebb current and residual tidal gyre.

---

## Highlights

► Channelised tidal currents in macrotidal environment induce large variation in dune migration rates across a dune field at the outlet of the Bay of Brest. ► Hydrodynamic forcing by tidal currents combining bi-directional currents in the channel and a tidal gyre in the shallower nearshore terrace allow the recirculation of sediment from dune field through external pathways. ► The location of the dune field *extending on the channel floor and along the steep side of the channel* shows the impact of varying bottom slopes on dune migration rates, with reduced rates on the negative slopes and increased rates on the positive slopes.

**Keywords** : sand body evolution, sediment transport, coastal sediment budget, hydro-geomorphological control

## 1. INTRODUCTION

40

41

42

43

44

45

46

47

48

49

50

51

52

53

54

55

56

57

58

59

60

61

Characterising the dominant direction and pathways of sediment transport in inner continental shelf and coastal systems is essential for defining the extension of sedimentary cells and the long-term sedimentary budget of coastal systems. The defining character of these systems is that wave shoaling and breaking induce a mean landward-directed bottom shear stress and, therefore, mean sand movement towards the shore (Allen, 1968). Nevertheless, the littoral energy fence can be bypassed by large amounts of material during shoreface erosion by storm wave processes, river floods, and ebb tidal enhanced currents as observed for estuarine and tide-dominated coastal systems as addressed in this paper (Allen, 1968; Swift, 1976; Barnard *et al.*, 2013; Fraccasia *et al.*, 2016; Preston *et al.*, 2018; Cruz and Noernberg, 2020). Overall, the assessment of sediment transfers, both cross-shore and longshore, between different components of the coastal system remains a major limitation in the understanding of the morphodynamics of nearshore and inner shelf sediment structures. This is partially due to the lack of high resolution datasets preventing full characterisation of coastal systems with seasonal variations of sedimentary fluxes (*e.g.* Ferret *et al.*, 2010) but also recirculation pathways as described in numerous tidal coastal systems (Elias and Hansen, 2013 ; Fraccascia *et al.*, 2016 ; Cruz and Noernberg, 2020). Nevertheless, sediment transport and sediment deposition, can be satisfactorily characterised by accurate monitoring of bedforms and other water-worked seabed features at the transition of shoreface and inner shelf. For instance, previous observations on submarine sand dunes have indicated a net seaward, regional scale, sediment transport in the San Francisco Bay coastal system, where tidal currents are enhanced by the inlet throat just inside Central Bay (Barnard *et al.*, 2012a and 2013).

62

63

64

65

66

67

68

69

A similar approach is adopted in this paper focusing on the sediment transport and identification of controlling factors at the outlet of a large tide-dominated estuary system sheltered from the open sea by a narrow bedrock tidal inlet: the Bay of Brest located in the most western part of Brittany (France). The study is based on the observation of submarine dunes field at the outlet of the Bay of Brest in Western Brittany (France) where water flows reaches up to 50,000 m<sup>3</sup>/s during spring tide. The detailed examination of these submarine dunes and the characterisation of their migration is carried out on an original dataset of bathymetric surveys acquired over the last 7 years, with seasonal to annual intervals. It offers opportunity

70 to better understanding short time scales ranging from seasonal to multiannual processes  
71 controlling sediment transport at the mouth of a highly energetic inlet system with the specific  
72 questions about the factors controlling dune migration, while also explaining the resilience of  
73 the dune system over time.

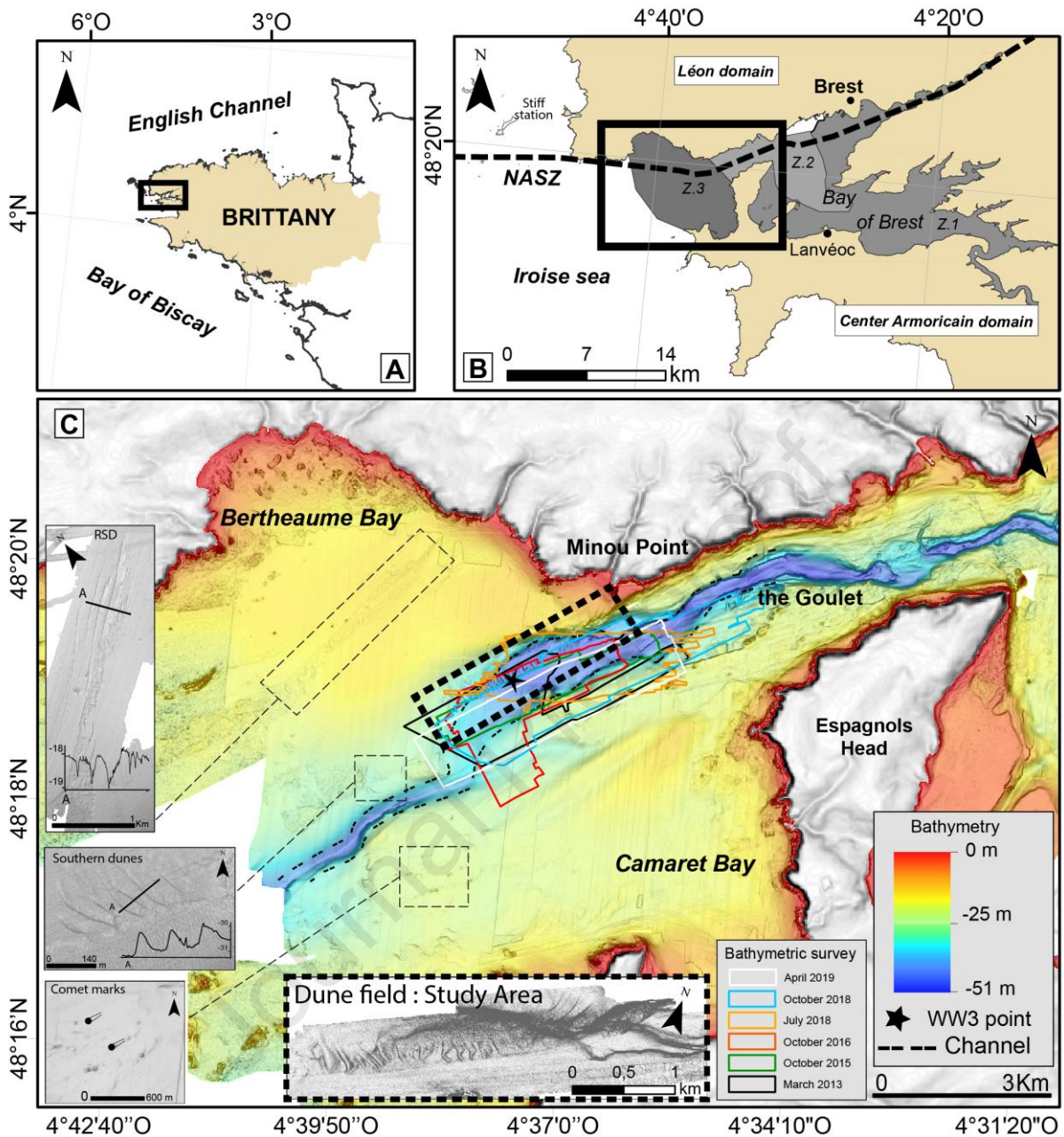
## 74 2. STUDY AREA

### 75 2.1. Geographical, geological and sedimentary setting

76 The study area is located at the outlet of the Bay of Brest at the western extremity of the  
77 Brittany Peninsula and in the northern extremity of the Bay of Biscay (Figure 1.A). The Bay of  
78 Brest is a semi-closed basin of about 181 km<sup>2</sup>, connected to the Iroise Sea by a relatively narrow  
79 channel (“The Goulet”) about 1.8 km wide and 6 km long and oriented NE-SW (Fichaut, 1989;  
80 Ballèvre *et al.*, 2009; Gregoire *et al.*, 2016). To the north side of the outlet, the water depth  
81 ranges from -10 m (relative to Lowest Astronomical Tide, LAT) near the Minou Point to -57 m  
82 (LAT) at the bottom of a buried paleo-channel system (Gregoire *et al.*, 2017).

83 This bay is characterised by three main sedimentary domains (Figure 1.B) (Gregoire *et*  
84 *al.*, 2016). First, the mud-prone estuarine domain in the upstream part of the bay (D1); mud is  
85 mixed in different proportions with other calcareous sediments. This upstream domain is fed  
86 by continental fluvial inputs. Second, the downstream part of the Bay (D2) characterised by  
87 mixed deposits composed of shelly, sandy gravel and pebbles. Finally, the sand-prone outlet of  
88 the Bay (D3) where the study area belongs. It is composed of sands (fine to gravelly) and shelly  
89 sands. This last domain exhibits a complex set of sedimentary features, including: i) a field of  
90 submarine sand dunes, this study focus, located on the right bank of the inlet at the outlet of the  
91 Bay of Brest (Figure 1.C. “Dune field: Study Area”) (Gregoire *et al.*, 2016). The granulometric  
92 signature of these dunes mainly consists of medium sand with high carbonate content (> 70%  
93 of total sediment weight); ii) another small dune field further west on the same bank of the  
94 channel. It is composed of 8 dunes which are between 0.5 m to 0.9 m high and their wavelength  
95 ranges from 24 m to 46 m (Figure 1.C. “Western dunes”). Their asymmetries are oriented from  
96 NE-SW; iii) a set of RSD (Ripple Scour Depression) located on the shallow platform extending  
97 northward of the D3 domain (the Bay of Bertheaume) (Figure 1.C. “RSD”) (Gregoire *et al.*,  
98 2016); iiiii) A comet marks field is also observed in the southern side of the channel, in Camaret  
99 Bay (Figure 1.C. “Comet marks”). The shape of these structures shown a dominate current  
100 oriented toward the NE due to sediment accumulation that occurred downstream of the  
101 obstruction.

102



103

104

105 Figure 1: A) Location of the study area in western Brittany; B) Close-up view of the study area  
 106 in the Bay of Brest and the Iroise Sea, D1: estuarine domain, D2: intermediate domain, D3:  
 107 external domain (Gregoire *et al.*, 2016) (NASZ: North Armoricain Shear Zone), Stiff station is  
 108 a meteorological station; C) Detailed map with six successive bathymetric surveys (period  
 109 2013-2019) of the study area, and other sedimentary bedforms reported by Gregoire *et al.*  
 110 (2016) (RSD: Rippled Scour Depression), the vertical scale of profiles is in meters, WW3 point  
 111 is a wave statistics node from WaveWatch III<sup>®</sup> model.

112

## 113 2.2. Hydrodynamic setting

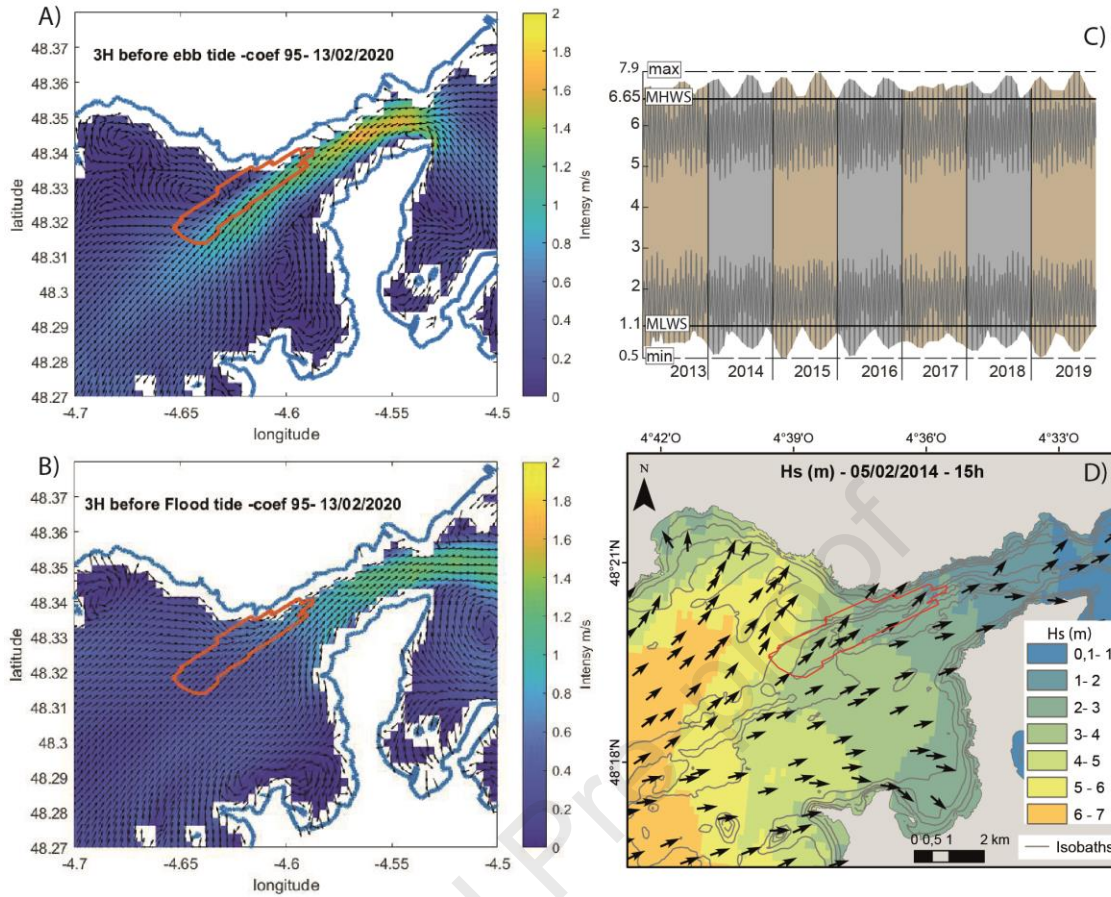
114 The tides are semi-diurnal with a tidal range varying from 1.22 m to 7.3 m. For spring  
 115 tide, the flow current oriented ENE, can reach 2 m/s in the Goulet and decreases in the bay of  
 116 Brest about 0.5 m/s. During the ebb period, the channel canalises the outflow and anticyclonic  
 117 gyres are formed in the Camaret, and Bertheaume bays. Ebb current speeds can reach a  
 118 maximum of 3.3 m/s at the Espagnols Head (SHOM, 1994). The analyses of MARS2D tide  
 119 model from Previmer for spring-tide level (Figure 2.A and 2.B) show a maximum flow can  
 120 reach 1.3 m/s during flood tide and 1.7 m/s during ebb tide in the Goulet. The tidal harmonic  
 121 analysis from 2013 to 2019 (Figure 2.C. and Table 1) indicate a minimum of 0.33 m for 2015  
 122 and a maximum of 7.28 m for 2015 and 2019. The hours exceeded 6.65 m (mean high water  
 123 spring) are 117 for 2016 and 2019 and 116 for 2015.

124 Data from WaveWatch III<sup>®</sup> model (Boudière *et al.*, 2013) for the period 2010-2016, for  
 125 a location in the Bay of Bertheaume over the studied dune field (-44 m depth; Figure 1.C for  
 126 localisation of WW3 node) indicate a swell direction at 80% WSW and 20% SW. The  
 127 significant wave heights range from 0.25 m to 2 m 90% of the time, and from 2 m to 4 m 7%  
 128 of the time. The same model indicates in storm conditions, for instance the 5 February 2014, a  
 129 swell direction from WSW and 4-5 m height at the west extremity of dune field and 2-3 m  
 130 height at the east extremity of dune field (Figure 2.D). During the last decade, several storms  
 131 were recorded in Brittany (Table 2) by Météo-France (official service of meteorology and  
 132 climatology in France). The 3 most morphogenetic storms have occurred during the 2013-2014  
 133 winter because they were combined with high spring tide levels (Blaise *et al.*, 2015).

134  
 135 Table 1: Tidal range statistics from 2013 to 2019 in meters. The “occurrence > 6.65 m”  
 136 indicate the number of hours that is exceeded for the mean high water spring level in  
 137 Bertheaume Bay.

Year	Median	Min	Max	Occurrence > 6.65 m
2013	3.81	0.60	7.07	103
2014	3.82	0.41	7.23	111
2015	3.82	0.33	7.28	116
2016	3.81	0.39	7.16	117
2017	3.80	0.57	6.97	110
2018	3.80	0.51	7.18	100
2019	3.81	0.34	7.28	117

138



139

140 Figure 2: A) and B) tidal current during ebb and flood tide on 13 February 2020 from Previmar  
 141 MARS2D tide model. C) The tidal harmonic from 2013 to 2019, the black lines represent the  
 142 mean high water spring (MHWS) and the mean low water spring (MLWS), the dashed lines  
 143 represent the maximum and minimum of the water level for the period 2013 to 2019 ; D) Wave  
 144 height (Hs) and direction from WaveWatch III<sup>®</sup> model (5 February 2014).

145 Table 2: Historical storms registered in Brittany between 2013 and 2019 (data from Météo-  
 146 France: [www.meteofrance.com](http://www.meteofrance.com); Blaise *et al.*, 2015; Previmar: <https://marc.ifremer.fr/> and Stiff  
 147 Station: <https://www.infoclimat.fr> )

Storm	Day-Month	Year	Ouessant Stiff Station (Km/h)	Wind direction	Wave Hs (mean) Iroise sea (m)	Wave Hs direction
<b>Dirk Noel</b>	23-25 December	2013	>100	S	5.54	SW
<b>Winter storms 2013-2014</b>	1-4 January	2014	114	SSW	6.13	W
	1-3 February	2014	150	W	6.04	W
	2-3 March 2014	2014	114	NNW	6.75	W
<b>Qendresa</b>	3-4 November	2014	>100	SW	3.07	W
<b>Zeus</b>	6-7 March	2017	190	NW	3.49	W
<b>Eleanor</b>	3 January	2018	126	W	6.00	W

148

### 3. METHODS

149

#### 3.1. Bathymetric Data

150

151

152

153

154

155

156

157

158

159

160

161

162

163

164

The analyses of dune morphology and sediment dynamics were done from bathymetric data acquired during six successive surveys realised by several institutions (Figure 1.C and Table 3). Bathymetric data were acquired using different multibeam echosounders (Table 3) with different GNSS (Global Navigation Satellite System) processing methods (Real Time Kinematic and Post Processed Kinematic). Data were processed using Qinsy-QPS software (IUEM data) and Globe software (IFREMER Data). The DTM of 2018 allowed to describe the morphology of the dunes with a resolution of 1 m. Dune migration was investigated at different time scales ranging from 4 and 6 months, 1 year, 2 years and 2.5 years, between March 2013 and April 2019.

Table 3: Configuration of survey acquisition systems (RTK: Real Time Kinematic; PPK: Post Processed Kinematic). DRASSM : Département des Recherches Archéologiques Subaquatiques et Sous-Marines; IFREMER : Institut Français de Recherche pour l'Exploitation de la MER ; IUEM/UBO : Institut Universitaire Européen de la Mer/Université de Bretagne Occidentale.

Survey Vessel	Institute	Date	acquisition system	DTM	vertical precision	horizontal precision	GPS treatment
Ess_dec_ata 19 Atalante	IFREMER	25-29/01/2019	Kongsberg EM710	1 m	1cm	1cm	RTK
Bertheaume Albert Lucas	IUEM/UBO	22-25/10/2018	Kongsberg EM3002	1 m	1cm	1cm	PPK
DRASSM André Malraux	DRASSM	02/07/2018	R2sonic 2024	1 m	1cm	1cm	PPK
Bertheaume Albert Lucas	IUEM/UBO	03-06/10/2016	Kongsberg EM3002	1 m	1cm	1cm	PPK
GeoLucas Albert Lucas	IUEM/UBO	27/10/2015	Kongsberg EM3002	1 m	1cm	1cm	PPK
Rebrade 2013 Thalia	IFREMER	03-07/03/2013	Kongsberg EM2040 D	2 m	1cm	1cm	RTK

165

166

#### 3.2. Data Analysis

167

168

169

170

171

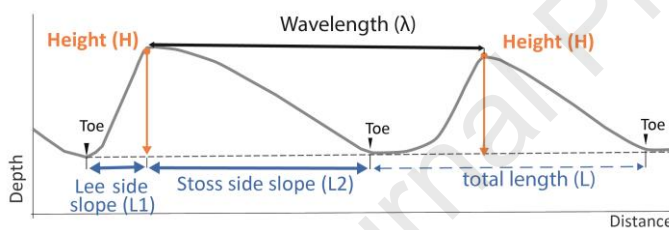
172

The morphodynamic dunes evolution results from the complex interaction between hydrodynamic conditions (tidal currents, swells, internal and storm waves), intrinsic sedimentary characteristics (lithology, grain size, amount of sediment available), and bedrock and sea level variations (Allen, 1968; Belderson *et al.*, 1982; Berne *et al.*, 1989 and 1993; Ashley, 1990; Idier *et al.*, 2002; Le Bot and Trentesaux, 2004; Ferret *et al.*, 2010). Therefore, it is essential to assess these morphological features by considering characteristic indexes



173 (height, wavelength, asymmetry...) to extract information about the surrounding environment  
 174 (Allen, 1980; Langhorne, 1982; Berne *et al.*, 1989 and 1993; Beck *et al.*, 1991). For example,  
 175 these measurements have been carried out on several dune fields in the Irish Sea to determine  
 176 the dune growth mechanisms in relation to tidal energy (Van Landeghem *et al.*, 2009 and 2012).

177 The morphological kinematic of the dunes is performed from the mapping of crests. As  
 178 developed in previous studies (*e.g.* Fraccascia *et al.*, 2016), the crest location is determined by  
 179 the zero-crossing analysis and the residual migration between surveys was measured using a  
 180 normal distance between crest displacements easy to identify from one year to another. The  
 181 characteristics of the dunes were determined by DTM analysis using two specific software: 1)  
 182 a GIS (geographic information system) software (ESRI™ ArcMap 10.6) to detect the crest of  
 183 the dunes and to measure their migration, and 2) a spreadsheet program (Microsoft™ Excel  
 184 2016) to calculate, analyse and plot data, including morphometric characteristics such as the  
 185 dune length or slope. Dune morphology was characterised using parameters and morphological  
 186 indices commonly used by marine sedimentologists (Figure 3) (*e.g.* Allen, 1980; Langhorne,  
 187 1982; Berne *et al.*, 1989).

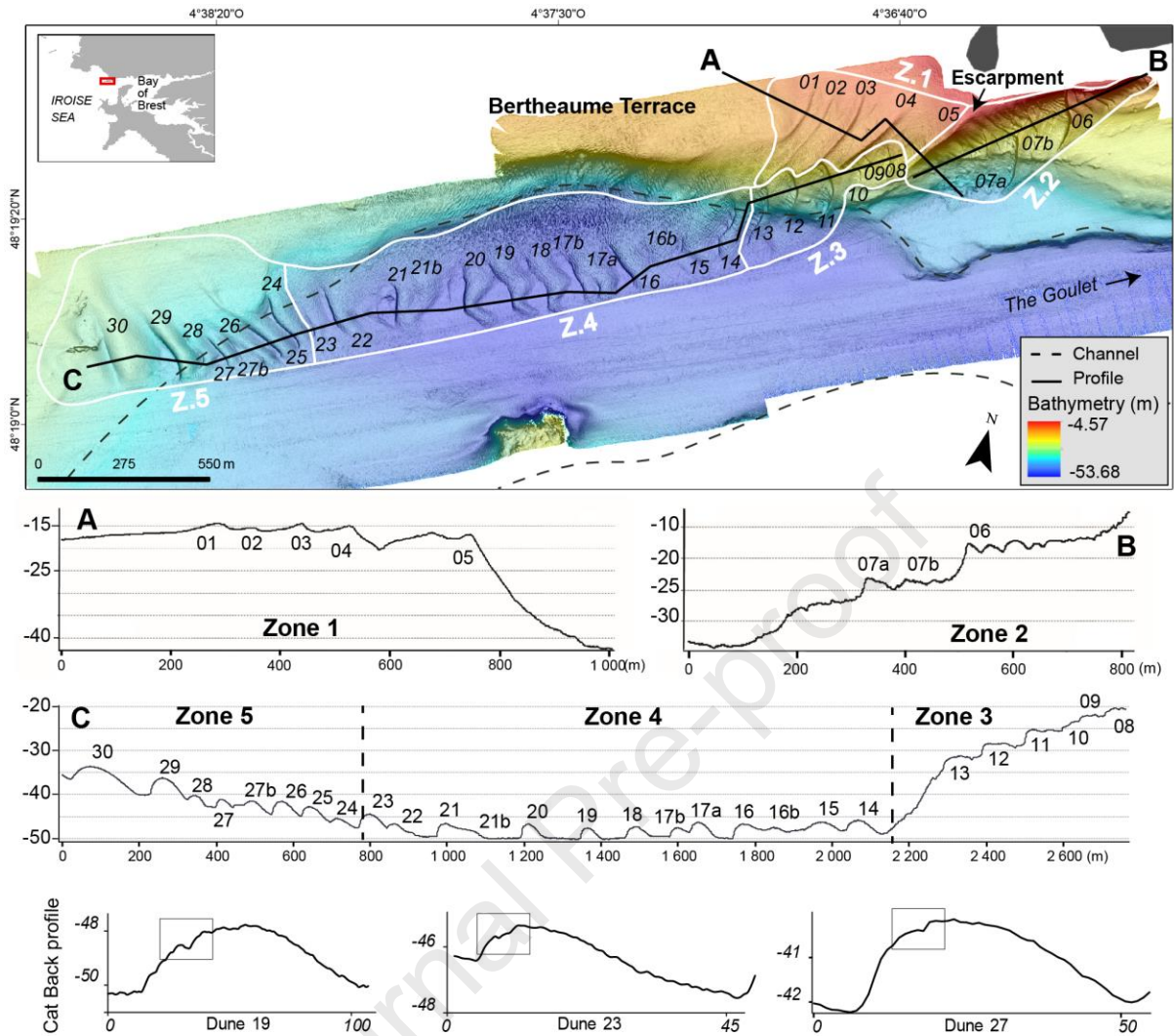


188  
 189 Figure 3: Morphological parameters of a transverse dune.

#### 190 4. RESULTS

191 Bathymetric data revealed that dune field is composed of 30 submarine dunes extending  
 192 southwestward over 3.5 km from the coastal headland Minou Point. Its lateral extension varies  
 193 from 250 m to 400 m wide; It borders the northern part of the inlet and spreads from an upper  
 194 terrace (the Bertheaume Terrace) from -10 m to -15 m to the deepest part of the inlet located at  
 195 -50 m (Figure 4).

196  
 197



198

199 Figure 4: Detailed map of the studied dune field and dune crests defined using (dunes 1-30,  
 200 grey lines) the October 2018 DTM with the cross-section profiles A, B, C and zones from Z.1  
 201 to Z.5 (Z. : zone). The profiles A, B, C illustrate the main morphological trends of the area. The  
 202 profiles of dunes 19, 23 and 27 represent the cat-back shapes. The axes of the profiles are in  
 203 meters.

#### 204 4.1. Partitioning of dune field

205 Considering the heterogeneous morphology of the area, characterised by significant  
 206 bathymetric variations ranging from -10 m to -50 m and the presence of the channel acting as  
 207 valley guiding and enhancing tidal currents, the study area was segmented into according to  
 208 characters of seafloor morphology: slopes, the water depth, location either on the terrace or  
 209 channel. These 5 zones were established as follows (Figure 4). The Zone 1 is located at the  
 210 northeast of the dune field, in the Bertheaume terrace, and includes dunes referenced 1 to 5,  
 211 which exhibits an asymmetry oriented from NW to SE. Dune 5, located at the edge of the

212 terrace, connects zones 1 and 2. Dune 5 lies on a bathymetric step at - 25 m, between the top  
213 and the toe of the escarpment (slope up to  $11^\circ$ ) corresponding to the northern edge of the  
214 channel. Zone 2 is located at the north-eastern end of the dune field and extends over the  
215 channel bank. It includes dunes 6 and 7 which exhibits an asymmetry oriented from NE to SW.  
216 These dunes are located on a steep slope of  $8^\circ$ . Zone 3 is located at the centre of the dune field  
217 along the toe of the channel bank. It includes dunes 8 to 13, which exhibits an asymmetry  
218 oriented from NE-SW. The average seafloor slope in zone 3 is  $10^\circ$ , inducing a 10 m variation  
219 of bathymetry over a length of 600 m. Zone 4 is located to the west of Zone 3, at a depth of  
220 about - 50 m corresponding to the deepest zone of the dune field and extends over a length of  
221 1500 m. Extending along the talweg of the channel, it includes dunes 14 to 23 which exhibits  
222 an asymmetry oriented from NE-SW. Zone 5 is located in the western most part of the dune  
223 field and is characterized by southwestward decreasing depth along the channel bank and range  
224 from - 41 m to - 33 m (slope:  $2.5^\circ$ ). It includes dunes 24 to 30 which exhibits an asymmetry  
225 oriented from NE-SW.

226

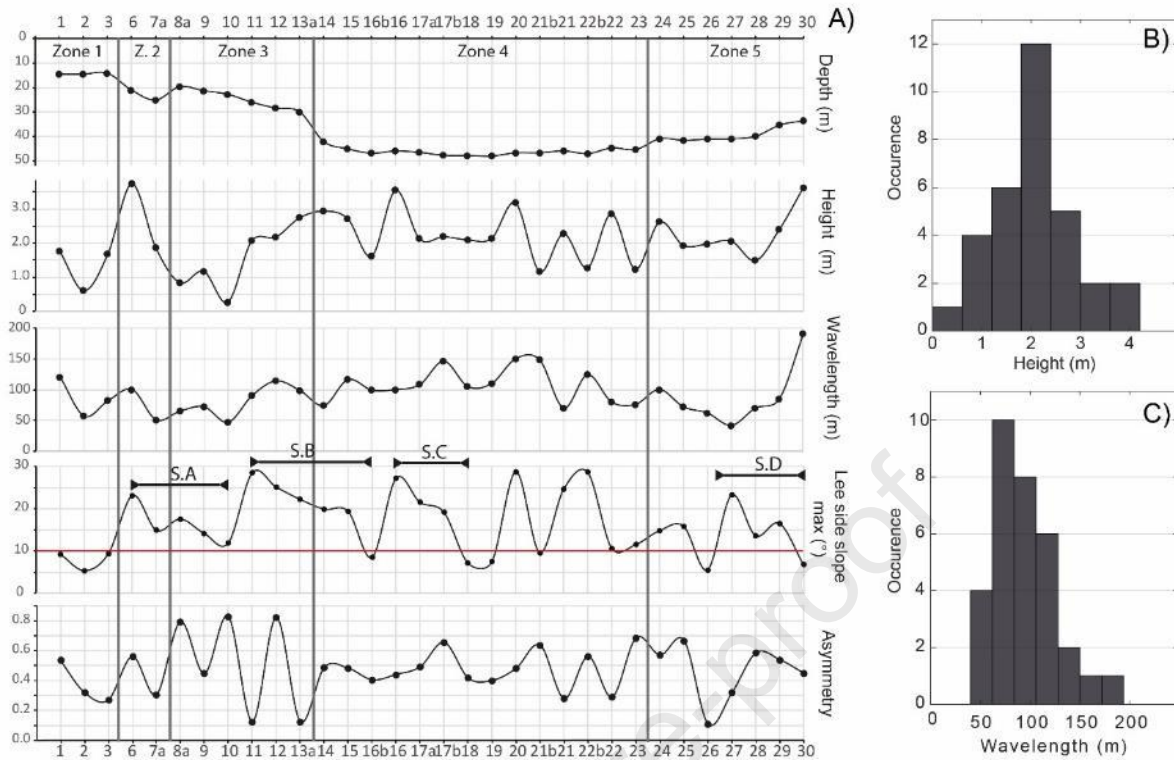
#### 227 **4.2. Morphology of dunes**

228 Morphological parameters are used to classify the dunes, determine their status (active or  
229 inactive) and evaluate their asymmetry (Allen, 1980; Knaapen, 2005). The morphological  
230 analysis of the dunes, based in October 2018 DTM, shows a high variability in their shape. The  
231 majority of dunes are between 0.5 m to 3.7 m high and their wavelength ranges from 10 m to  
232 190 m long (Figure 5). More specifically, one third of the dunes are between 2 m and 2.5 m  
233 high, and half of them are between 60 m and 100 m long.

234 In this study, the angles of the lee side fluctuate between  $5^\circ$  and  $30^\circ$  with a median around  
235  $15.3^\circ$ . Regardless of the zones, a consistent pattern of lee slide slopes can be observed, which  
236 concerns 4 groups of 4 or 6 dunes forming successive sequences note S.A to S.D (Figure 5.A).  
237 These sets of dunes show gradual morphological changes, starting from a maximum angle and  
238 decreasing to a minimum value before reconstructing a new sequence. In each sequence, from  
239 east to west (direction of migration of the dunes), the significant slope values of the lee side  
240 ( $25^\circ$ -  $35^\circ$ ) decrease until about  $10^\circ$ . The sequences are identified as follows with the index of  
241 dunes: S.A: [6-10]; S.B: [11-16b]; S.C: [16-18]; S.D: [27-30].

242

243



244

245 Figure 5: (A) Morphological characteristics (height, wavelength, lee side slope, and  
 246 asymmetry) of the dunes 1 to 30, and water depth above the crest. The continuous lines are  
 247 interpolations across the dune field along the profiles A to C. The red line on the plot shows the  
 248 lee-side slope corresponds to a  $10^\circ$  slope, considered as the limit between inactive and active  
 249 dunes (Belderson *et al.*, 1982). The sequences S.A, S.B, S.C, and S.D describe a slope trend  
 250 (lee side slope part). (B) and (C) Histograms of dune height and wavelength, respectively.

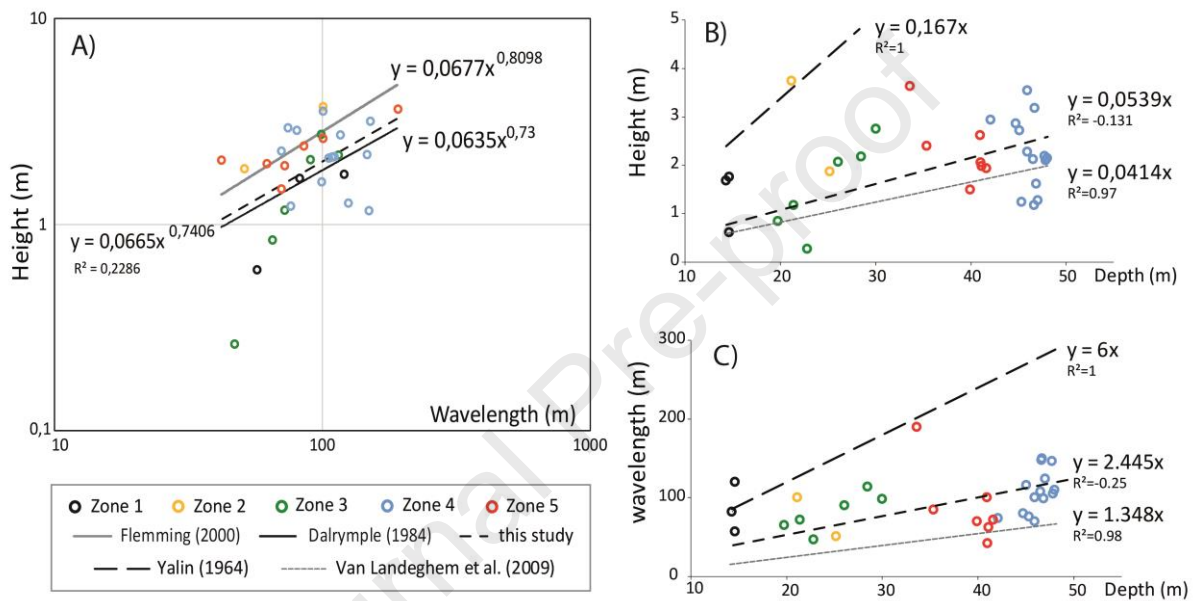
251 Dune asymmetry was calculated according to the formula of Knaapen (2005)  $[(L2-L1)/L]$   
 252 (Figure 3). For the dune field considered, asymmetry fluctuates between 0.1 and 0.8 (an average  
 253 of 0.5) and shows a narrow range of variations between dunes 14 and 25, with asymmetry  
 254 values contained within the range 0.3-0.7 (Figure 5.A). Dunes 6-8-10-12-17b-21b-23-25, have  
 255 an asymmetry index above the maximum value of 0.6 measured by Van Landeghem *et al.*  
 256 (2012) in the Irish Sea.

257

### 258 4.3. Height vs wavelength

259 In this study, the results obtained (Figure 5.A) show that height and wavelength seem to  
 260 be well correlated in most parts of the field but presented in reality rapid fluctuations from one  
 261 dune to another. The results, in terms of the distribution of heights and wavelengths of the study  
 262 area, are very similar to these of Flemming (2000) and Dalrymple (1984), but the coefficient of

263 determination is rather small ( $R^2= 0.2$ ) (Figure 6.A). Dunes within each zone seem to follow  
 264 somewhat distinct correlation patterns (Table 4). In zones 1 and 3, with  $R^2$  of 0.77 and 0.91  
 265 respectively, there is a good correlation between  $H$  and  $\lambda$ , noting that the exponent is higher  
 266 than in the literature. Zone 2 is not evaluated for this rating because it comprises only two  
 267 points. In zone 4, with the coefficient of 0.02, the correlation is very poor. In zone 5, the  
 268 coefficient of determination (0.6) indicates an intermediate correlation between  $H$  and  $\lambda$ , with  
 269 an exponent that remains lower than in the literature.  
 270



271  
 272  
 273 Figure 6: (A) Scatter plot of dune height *versus* wavelength with colours by zones of the dune  
 274 field. Power law regressions and variance coefficients for each zone are summarised in Table 4.  
 275 Power laws between dune dimensions and water depth compared with Van Landeghem *et al.*  
 276 (2009) and Yalin (1964) observations; (B) Dune height *versus* water depth; (C) Dune  
 277 wavelength *versus* water depth.

278  
 279 Table 4: Power law regressions of dune height *versus* wavelength (Figure 10) and coefficients  
 280 of determination for zones 1 to 5.

Zone	Equation	$R^2$
1	$H= 0.0023*\lambda^{1.4247}$	0,77
2	$H= 0.0322*\lambda^{1.0322}$	1,00
3	$H= 0.00002*\lambda^{2.5864}$	0,91
4	$H= 5.1988*\lambda^{-0.194}$	0,02
5	$H= 0.2855*\lambda^{0.4674}$	0,60

281

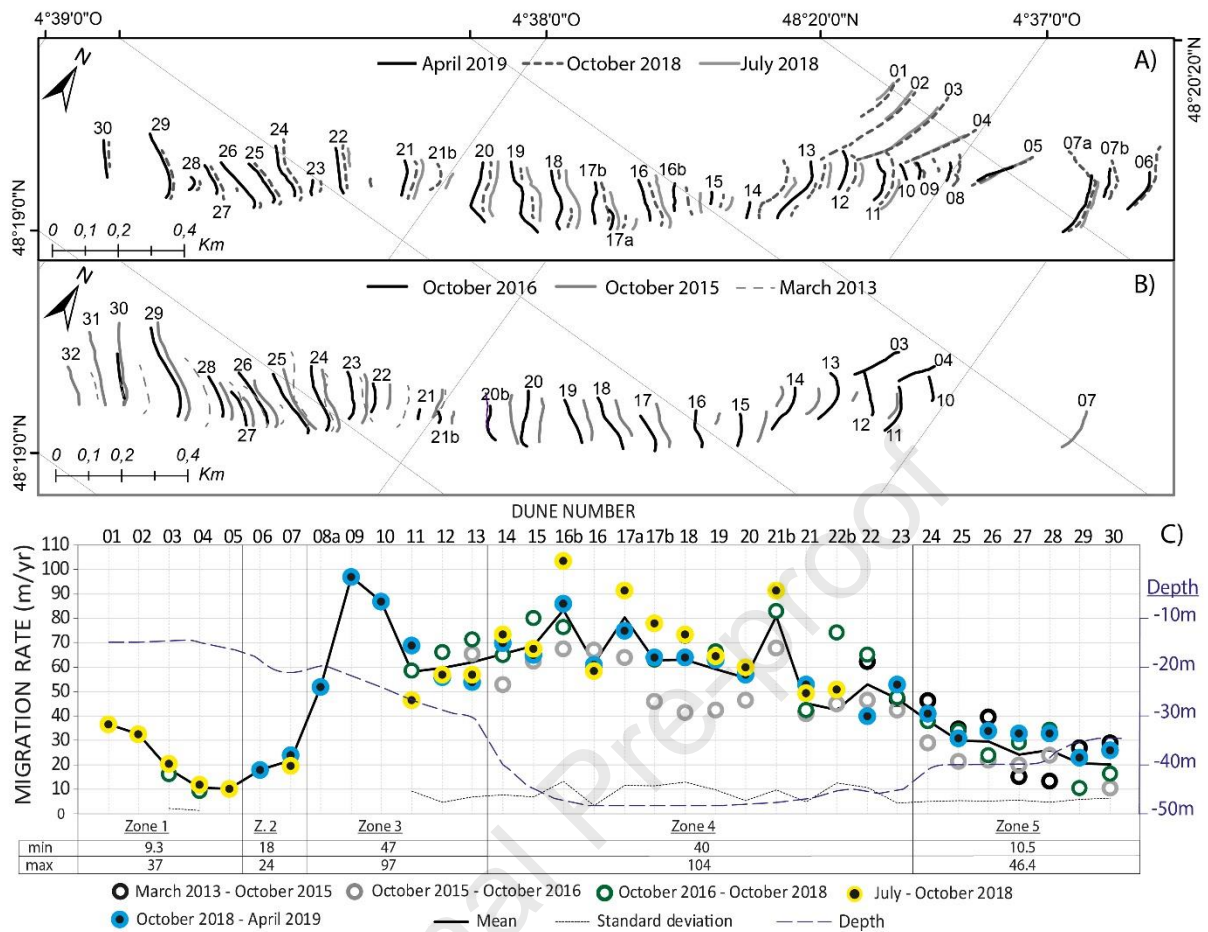
#### 282 4.4. Height or wavelength vs depth

283 Prior studies on other dune fields report an increase in dune height with increasing water  
 284 depth (Yalin, 1964; Besio *et al.*, 2006; Van Landeghem *et al.*, 2009; Blondeaux and Vittori,  
 285 2011; Van Santen *et al.*, 2011; Reynaud and Dalrymple, 2012). In this study, the relationship  
 286 between dune height and water depth over the whole dune field is given by the power law  $H =$   
 287  $0.0539 \cdot D$  (Figure 6.B), which is close to the equation obtained by Van Landeghem *et al.* (2009)  
 288 in the Irish Sea, but with a very low  $R^2 = 0.08$ . The dune wavelength to water depth power law  
 289 in this study corresponds to  $\lambda = 2.445 \cdot D$  (Figure 6.C), which is also close to the equation  
 290 obtained by Van Landeghem *et al.* (2009) in the Irish Sea. In zones 1 and 4, there is a range of  
 291 dune height and wavelength whereas the depth remains nearly constant. In zone 3, where the  
 292 bathymetry varies from -20 m to -30 m, there appears to be a good correlation between the  
 293 increase in dune height and the increase in depth ( $R^2 = 0.97$ ; dune 10 is excluded because it is  
 294 less than 0.5 m high). A similar strong correlation appears between  $\lambda$  and depth in zone 5, where  
 295 the dunes migrate upslope (from -41 m to -33 m); the regression analysis (with  $R^2 = 0.54$ )  
 296 suggests decreasing dune height and wavelength with increasing water depth.

#### 298 4.5. Dune migration

299 The dunes show different migration rates depending on the zone considered (Figure 7).  
 300 At the scale of the dune field, there is an inverse relationship between migration rate and water  
 301 depth. Dunes in zones 3 and 4 migrate very rapidly, around 60 m/yr, while dunes in zones 1, 2  
 302 and 5 migrate slower, around 20 m/yr. Considering these rates, it would take about 70 years for  
 303 a dune initially positioned at the end of zone 3 to exit the system (end of zone 5). Considering  
 304 each zone individually, the following trends can be noted. In zone 1, the rate decreases from  
 305 dune 1 to dune 5 (from 37 m/yr to 10 m/yr, based on the July-October 2018 datasets). In zone 2,  
 306 the only available data (October 2018 and April 2019) shows that the migration rate increases  
 307 from dune 6 to dune 7 (from 18 m/yr to 24 m/yr). In zone 3, the speed of migration tends to  
 308 increase lightly from 60 m/yr to 70 m/yr, except for dunes 9 and 10 considering the April 2019  
 309 dataset. From part of zone 3 and in most of zone 4, from dunes 11 to 20, the migration rate is  
 310 relatively homogeneous, around 60-70 m/yr. From dune 21 to the western end of the dune field  
 311 (rest of zone 4 and zone 5), the migration rate decreases to reach a low average value of around  
 312 10 m/yr. The migration rate is consistent across all investigated time scales (4-6 months, 1-2-  
 313 2.5 years), with a standard deviation varying from 1.3 m/yr to 12.7 m/yr (7.2 m/yr on average)  
 314 over the whole area, and without outliers.

315



316

317

318

319 Figure 7: Migration of dune crests between (A) April 2019, October 2018 and July 2018 and  
 320 (B) between March 2013, October 2015 and 2016; (C) Yearly migration rate according to the  
 321 dune number (1 to 30) across the five zones. The black line represents the mean migration rate  
 322 (m/yr) and the dotted line is the standard deviation per dune for different periods under  
 323 consideration. The dashed line is the water depth.

324 The trends observed within each zone in a given year can also be seen in other years,  
 325 except the high migration rate of dune 9 (97 m/yr) and 10 between October 2018 and April  
 326 2019, and the low migration rate of dunes 17b to 20 between October 2015 and 2016. The  
 327 dataset allows examining seasonal effects on dune migration rates. Migration rates between  
 328 July and October 2018 correspond to the summer period (yellow symbol), while migration rates  
 329 from October 2018 to April 2019 correspond to winter period (blue symbol). At this seasonal  
 330 time scale, focusing on dunes 12 to 20 (zones 3 and 4), results suggest that the migration rate is  
 331 systematically higher during the summer period (on the order of a few m by year). This

14

332 seasonality in the migration rate is only noticeable in the central dune field (zones 3 and 4),  
333 which also corresponds to the deepest part of the dune field, in the channel bottom. Although  
334 here the migration rates are consistent across all investigated time scales, as was just noted,  
335 these results, derived from a summer to winter comparison over a single year, should be  
336 confirmed using a longer time series with bathymetric surveys acquired twice a year.

## 337 5. DISCUSSION

338 The morphodynamic characterisation of the dune field obtained through the interpretation  
339 of successive bathymetric DTMs shows that this nearshore submarine dune system changes  
340 over short distances, and is correlated with the seafloor morphology. The observed variability  
341 of forms and dynamics is analysed considering all the hydrodynamic and sedimentary factors.

342

### 343 5.1. Dune field morphology and equilibrium conditions

344 According to the classification of Berne *et al.* (1989), these sediment waves can be  
345 categorised as large to very large dunes. They are comparable to the dunes identified in other  
346 macrotidal coastal environments such as the Gironde estuary (Berne *et al.*, 1993; Mallet *et al.*,  
347 2000) or Arcachon channel (Thauront *et al.*, 1996), where dune heights vary between 1.6 m and  
348 4.2 m and wavelengths between 58 m and 107 m. Submarine dunes with similar characteristics  
349 have also been observed in the shallow inner shelf (between -20 m to -40 m depth) and in the  
350 macrotidal context of the Pas de Calais Strait by Berne *et al.* (1989) and Le Bot and Trentesaux  
351 (2004). It is also the case for the Bay of San Francisco corresponding to another case of a highly  
352 energetic inlet system (Elias and Hansen, 2013) where dune size is similar to that of this present  
353 study at the same depth. Thus, dune size (height and wavelength), observed at the outlet of the  
354 Bay of Brest, is consistent with most of dune size case studies reported in examples of tidal  
355 coastal environments. Nevertheless, the "generally-accepted" correlation between dune height  
356 with wavelength and related power-laws (Allen, 1968; Dalrymple, 1978; Flemming, 2000;  
357 Francken *et al.*, 2004) are not systematically applicable to the present case study. Thus, the  
358 analyses of the geometrical relationship between  $\lambda$  and H, suggest that deeper (< -20 m) dunes  
359 (Z1 and Z2 areas) and those observed in steep slope (Z3 and Z5 areas) approach an equilibrium  
360 state. In contrast, the dunes located in the deepest part of the channel (Z4 area) where tidal  
361 currents are assumed to enhance by constriction of water flow are far from that equilibrium.

362 Prior studies on dune fields (*e.g.* Yalin, 1964) and recent works devoted to the process of  
363 the formation of tidal dunes have shown that predictions of the wavelengths of tidal dunes are  
364 strongly dependent on the mean water depth (Besio *et al.*, 2006; Blondeaux and Vittori, 2011;



365 Van Santen *et al.*, 2011). Nevertheless, some authors indicate that correlation is not always  
366 clear (Dalrymple, 1978; Flemming, 1978; Ashley, 1990; Van Landeghem *et al.*, 2009; Ferret *et*  
367 *al.*, 2010) and suggest examining these predictions in relation to the studied coastal system. In  
368 this study, the good correlation between dune size and water depth, obtained in steep north flank  
369 of the channel (zones 3 and 5) suggests that a significant gradient in the bathymetry can play  
370 an important role in controlling dune growth. In contrast, zones 1 and 4 corresponding to a more  
371 planar seabed, show poor correlation between sizes of dunes and water depths. This result  
372 suggests that water depth is not a key control factor of dune grows on the planar area; it is  
373 probably more dependent on the variability of tidal currents in the deep and narrow inlet.

374 The morphology of the inlet is also involved in the control of lateral extension of dunes.  
375 Indeed, despite similar hydrodynamics settings, lateral extension of dunes is much greater in  
376 the mouth of San Francisco Bay where it reaches up to 1000 m (Elias and Hansen, 2013) than  
377 in the external domain of Bay of Brest (450 m). The main difference between these two mouths  
378 is the presence of a very marked paleochannel at the inlet of the Bay of Brest, in contrast to  
379 mouth of San Francisco Bay, where the bathymetry remains flatter. Thus, the presence of this  
380 well-marked incised valley limits the lateral extension of dunes.

381 In this study, the dunes generally show a very well-marked asymmetry (an average of  
382 0.5), which is a signature of a single dominant current direction affecting dune morphology  
383 (Allen, 1980). However, in zones 4 and 5, most dunes have a cat-back profile, possibly  
384 indicative of a subordinate current in the opposite direction to the tidal residual current, and  
385 strong enough to reshape the top portion of the dune and smooth the dune crest.

386

## 387 **5.2. Dunes migration**

388 The measured migration rates show ample variations in space and time, with values  
389 ranging from 10 m/yr to 70 m/yr. According to the synthesis by Thauront *et al.* (1996),  
390 submarine dune migration rates measured in this study are similar to those described in the  
391 literature (e.g. Langhorne, 1973 and 1982 and Berne *et al.*, 1989 b).

392 However, lee side slope patterns observed in October 2018, for several dunes (1, 2, 3,  
393 16b, 18, 19) show values below  $10^\circ$  suggesting that the latter are not active (Belderson *et al.*  
394 1982); however the migration rate records for these dunes are higher than 30 m/s between 2015  
395 and 2019, show that the latter are mobile on a pluri-annual and seasonal scale. Moreover the  
396 apparent immobility of these dunes is difficult to be considered as stable over time in regard to

397 the mobility of direct adjacent dunes. In consequence, the apparent inactivity of some dunes  
398 could rather be interpreted as a stationary state for a given period of time.

399 Changes in migration rates as a function of dune size, in zones 3 and 5, do not verify the  
400 classical inverse relationship, where migrating velocity is inversely proportional to the dune  
401 height and consequently to the dune size (e.g., Charru *et al.*, 2013). This atypical behaviour can  
402 be discussed in the light of the morphology of the seafloor and associated hydrodynamics. In  
403 zone 3, the increase of migration rate is correlated with water depth. Similarly, in zone 5, the  
404 decrease of migration rate is observed to occur concomitantly with a decrease in water depth.  
405 For this latter zone, the seafloor slope is opposite to the migration direction, and expected to  
406 reduce the sediment transport rate. It is thus clear that the gradient of the seabed slope acts as a  
407 significant factor modulating the migration rate of dunes according to its orientation opposite  
408 to the same direction as dunes displacement. Moreover, the results also suggest that orientation  
409 of the bottom slope gradient has more influence on variations of migration rate than dune size.  
410 Thus, once the slope gradient of seabed is significant, the classical inverse relationship (height  
411 versus migration rate dunes) is not observed and the slope of the basal surface of dune migration  
412 controls the migration rate.

413

### 414 **5.3. Control factors at different time scales**

415 The tidal circulation appears to be the main factor controlling the direction of dune  
416 migration. Indeed the results show that the NE-SW migration direction of the dunes in  
417 channelised part (zones 2 to 5) is conformed to the ebb current orientation. At the opposite, out  
418 of the channelised part, the NW-SE current pattern along the Minou point is responsible for the  
419 direction of dune migration along the zone 1 whatever the flood or ebb periods. In this way, the  
420 dunes observed in the terrace (zone 1) are shaped by a residual current oblique to the main  
421 transport observed in the inlet. As shown by the current pattern (Figure 2.A), the dunes  
422 migration and sediment transport located to the north of the inlet are induced by a clockwise  
423 gyre extending over the shallow Bertheaume Bay. Other studies of tidal channels show that  
424 these residual circulation gyres, positioned tips of the channel, are quite common and control  
425 the dune morphology that is maintained stable over time with a continuous recycled sand flux  
426 (Cruz and Noernberg, 2020 and Fraccasia *et al.*, 2016).

427 From seasonal to annual scale, several authors noted that hydrodynamic agents such as  
428 tidal fluctuations and storms (waves and currents) can temporarily modify migration rates and  
429 even reverse migration directions (Grochowski *et al.*, 1993; Van Dijk and Kleinhans, 2005; Le

430 Bot *et al.*, 2000 and 2006; Idier *et al.*, 2002; Le Bot and Trentesaux, 2004; Ferret *et al.*, 2010).  
431 Several hypotheses may explain variations in migration rates observed from one year to the  
432 next, with notably lower velocities between October 2015 and October 2016 (about 10 m/yr  
433 less than in other years). A first hypothesis is the effect of yearly variations in extreme tidal  
434 ranges and associated tidal currents. Larger would be the tide range, greater would be the shear  
435 stress on the seabed during ebb and flood. The comparison of tidal ranges over the period 2013-  
436 2018 shows that tidal ranges were largest in 2015-2016, implying higher transport capacity,  
437 associated tidal current velocities. This stronger bed shear stress of subordinate current (flood),  
438 occurred during the high string tide level, has a higher ability to slow down the progression of  
439 the dunes. Hence, variations of annual tidal range seem to have an impact on the annual rate of  
440 dune migration. Another hypothesis is that storm winds and high swells are able to remobilise  
441 sediments and reverse the direction of migration (Van Dijk and Kleinans, 2005; Le Bot *et al.*,  
442 2000 and 2006; Idier *et al.*, 2002; Le Bot and Trentesaux, 2004; Ferret *et al.*, 2010). From 2015  
443 to 2016, the French weather service (Météo-France) does not indicate any major storms. During  
444 the last decade, the most severe storms that impacted the Brittany coast, occurred during the  
445 winters of 2013-2014 and 2017. Unfortunately, the dataset lacks DTM in 2014 and 2017, which  
446 makes it unlikely to measure the direct effect of these storms on the morphodynamics of the  
447 dune field.

448 Over a tidal cycle, the macrotidal context of the Bay of Brest and the flow acceleration  
449 due to the narrow inlet is also susceptible to have a predominant role in the morphogenesis of  
450 the dunes. In this study, cat-back shapes were observed on some dunes located in the channel  
451 and may indicate the presence of subordinate currents opposite to the residual flow (McCave,  
452 1971). Doré *et al.* (2017) showed that the flood current (here, the subordinate current) induces  
453 cat-back shapes on the morphology of tidal dunes in the Arcachon Channel. The same process  
454 occurs in the Bay of Brest, during spring flood, when the current velocity can reach 0.8 m/s,  
455 above the 0.5 m/s threshold necessary for dune initiation. At this study site, the reverse current  
456 (flood) is further enhanced by the channelised context (-50 m water depth) and is strong enough  
457 to remobilise the sediment to the dune crest, thus providing cat-back shape.

458

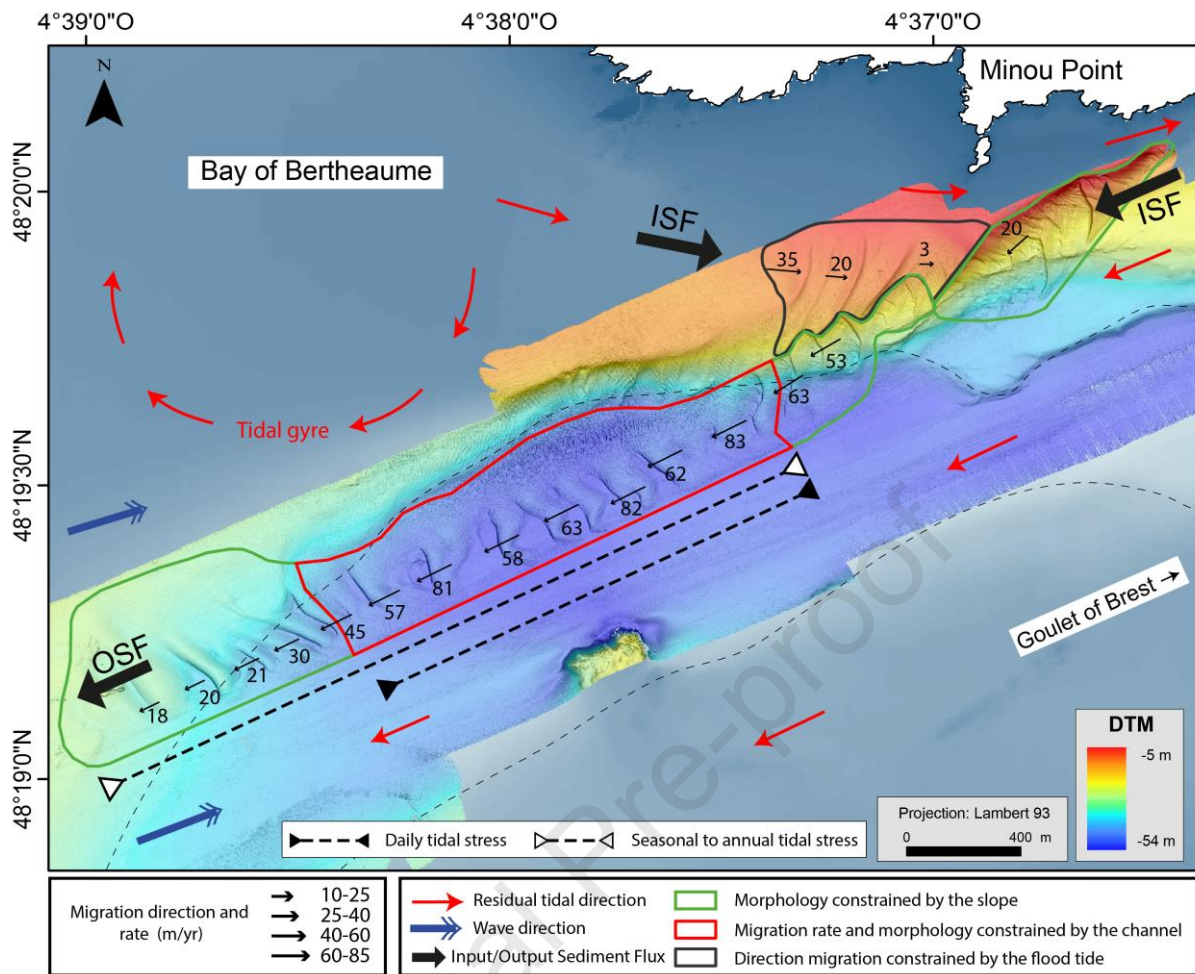
#### 459 **5.4. Sediment transport patterns**

460 Several sediment sources and sinks can be identified in the studied dune field. Material  
461 input occurs through the eastern and northeastern shallow end of the field and is controlled by  
462 the ebb and flood current. The exit of material occurs toward the southwestern deeper part of

463 the channel (Figure 8). Overall, the migration of dunes indicates a steady-state net seaward sand  
464 transport at the outlet of the Brest Bay coastal system. The small western dune field, with an  
465 asymmetry oriented toward the SW confirm the net sediment transport toward the exit of the  
466 Bay of Brest and the Iroise Sea. Moreover, the tidal Bay of Bertheaume gyres, close to the  
467 channel and the field dune northwestern input (ISF in Figure 8), provide that a recirculation  
468 sediment loop can occur between this major dune field and the bay of Bertheaume and RSD.  
469 This indicated the presence of a little sediment cell in the middle of this embayment in  
470 connection with the northern flank of the tidal channel. In the southwestern part of the external  
471 domain relating to Camaret Bay, the outflow seems to be compensated by the flood current as  
472 suggested by the presence of comet marks oriented to the NE. However, the few sedimentary  
473 structures in this southern part suggest a more limited sediment transport.

474         What about other similar documented examples? The greatest similarity is with the mouth  
475 of San Francisco Bay, which is a similar macrotidal environment and almost identical mouth  
476 morphology due to the presence of an inlet channel opened onto two embayments on each side.  
477 According to Elias and Hansen (2012), the flow current (ebb and flood) at the exit of the San  
478 Francisco bay, produce residual tidal gyres in the embayments. Carefully, in San Francisco  
479 external domain, the recirculation eddy contribute to the beach stability. The same process  
480 occurs in the Bertheaume Bay where the ebb and flood gyres contribute to the recycling of  
481 sediment dunes. Thus, for both channel inlets subjected to reverse tidal currents, the  
482 recirculation eddy due to hydro-morphology context of these mouths (inlet channel opened into  
483 two embayments on each side), induce stability of sedimentary cells.

484



485  
 486 Figure 8: Conceptual diagram of dune field system in relation to residual tidal currents and  
 487 waves. Areas where dune morphology is constrained by slope of seabed (green), the flood tide  
 488 (black) and the ebb tide in the deep channel (red). The Sediment Flux Inputs (ISF) and Outputs  
 489 (OSF) are also indicated.

## 490 6. CONCLUSIONS

491 This paper presents a submarine sand dunes morphodynamic monitoring at both the  
 492 seasonal and pluriannual scales, which allows for defining the sediment transport pathway. The  
 493 analysis of the dune morphology and migration rate has highlighted several characteristics as  
 494 follows:

495 The sizes of the dunes, observed at the outlet of the Bay of Brest, is consistent with  
 496 previous studies related to tidal coastal environments. However, the equilibrium of the dunes is  
 497 only obtained in the deepest zones, above -30 m and in steep slopes area. This narrow inlet  
 498 channel, exposed to the tidal current, prevents the usual development of the dunes below depth  
 499 of 15 m. Water depth is not a significant control factor for dunes growth which is more  
 500 dependent on the disparity of tidal currents through the deep and narrow channel.

501 In this macrotidal context, the ebb current appears the main factor that control the rate  
502 and direction of dunes migration. The flood current could be the origin of a decrease in the  
503 migration rate during higher tidal range periods, due to an increase in the shear stresses on the  
504 seabed in the opposite direction of migration. The second factor controlling morphology and  
505 migration rate is the seabed morphology specifically the strongly incised channel and these  
506 steep slopes. Indeed, the slope gradient of the seabed also acts as a significant factor modulating  
507 the migration rate and limiting the lateral extension of dunes.

508 Finally, the morphodynamic analysis of this dune field has revealed that the sediment  
509 transfers at the Bay of Brest mouth are mainly oriented toward the Iroise Sea. However, a  
510 circular sediment cell has been identified between the embayment and the inlet channel in  
511 relation to the tidal gyres. Thus, part of the sedimentary material supplying the dune field would  
512 be recycled by this tidal gyre. Subsequently, it would be interesting to carry out sediment  
513 transport modelling to improve these results. The study of dune morphodynamics has therefore  
514 allowed us to improve our knowledge of sediment transport, an essential key to understanding  
515 the management of marine human activities.

516

#### 517 **Declaration of competing interest**

518 The authors declare that they have no known competing financial interests or personal  
519 relationships that could have appeared to influence the work reported in this paper.

520

#### 521 **Acknowledgments**

522 The authors would like to thank the crew of Research Vessel Albert Lucas, Marcaurélio  
523 Franzetti, Mickaël Beauverger and Christophe Prunier (LGO engineers) for their contribution  
524 to data collection, the “Département des recherches archéologiques subaquatiques et sous-  
525 marines (DRASSM)” for providing us with the bathymetric dataset of July 2018, Hervé  
526 Bisquay (Hydrographer in charge of data quality at Genavir) for providing us bathymetric with  
527 the dataset of April 2019, and Stephane Bertin for his careful proofreading.

528

#### 529 **References**

- 530 Allen, J.R.L., 1968. The Nature and Origin of Bed-Form Hierarchies. *Sedimentology* 10, 161–  
531 182. <https://doi.org/10.1111/j.1365-3091.1968.tb01110.x>
- 532 Allen, J.R.L., 1980. Sand waves: A model of origin and internal structure. *Sedimentary Geology*  
533 26, 281–328. [https://doi.org/10.1016/0037-0738\(80\)90022-6](https://doi.org/10.1016/0037-0738(80)90022-6)

- 534 Ashley, G.M., 1990. Classification of large-scale subaqueous bedforms; a new look at an old  
535 problem. *Journal of Sedimentary Research* 60, 160–172. <https://doi.org/10.2110/jsr.60.160>
- 536 Ballèvre, M., Bosse, V., Ducassou, C., Pitra, P., 2009. Palaeozoic history of the Armorican  
537 Massif: Models for the tectonic evolution of the suture zones. *Comptes Rendus Geoscience*  
538 341, 174–201. <https://doi.org/10.1016/j.crte.2008.11.009>
- 539 Barnard, P.L., Erikson, L.H., Rubin, D.M., Dartnell, P., Kvittek, R.G., 2012a. Analyzing  
540 bedforms mapped using multibeam sonar to determine regional bedload sediment transport  
541 patterns in the San Francisco Bay coastal system. In: Li, M.Z., Sherwood, C.R., Hill, P.R.  
542 (Eds.), *Sediments, Morphology and Sedimentary Processes on Continental Shelves: Advances in Technologies, Research and Applications: International Association of*  
543 *Sedimentologists (IAS) Special Publication 44*, pp. 272–294.
- 545 Barnard, P.L., Schoellhamer, D.H., Jaffe, B.E., McKee, L.J., 2013. Sediment transport in the  
546 San Francisco Bay Coastal System: An overview. *Marine Geology* 345, 3–17.  
547 <https://doi.org/10.1016/j.margeo.2013.04.005>
- 548 Beck, C., Clabaut, P., Dewez, S., Vicaire, O., Chamley, H., Augris, C., Hoslin, R., Caillot, A.,  
549 1991. Sand bodies and sand transport paths at the English Channel-North Sea border:  
550 Morphology, dynamics and radioactive tracing. *Oceanologica Acta* 11, 111–121.
- 551 Belderson, R.H., Johnson, M.A. and Kenyon, N.H., 1982. Offshore tidal sand. In: Stride, A.H.  
552 (Eds.), *Processes and deposits*. Chapman and Hall Ltd, London, pp. 27-57.
- 553 Berne, S., Allen, G., Auffret, J.P., Chamley, H., Durand, J., Weber, O., 1989. Essai de synthese  
554 sur les dunes hydrauliques geantes tidales actuelles. *Bulletin de la Société Géologique de*  
555 *France* V, 1145–1160. <https://doi.org/10.2113/gssgfbull.V.6.1145>
- 556 Berne, S., Castaing, P., Drezen, E.L., Lericolais, G., 1993. Morphology, internal structure, and  
557 reversal of asymmetry of large subtidal dunes in the entrance to Gironde Estuary (France).  
558 *Journal of Sedimentary Research* 63, 780–793. <https://doi.org/10.1306/D4267C03-2B26-11D7-8648000102C1865D>
- 560 Besio, G., Blondeaux, P., Vittori, G., 2006. On the formation of sand waves and sand banks.  
561 *Journal of Fluid Mechanics* 557, 1–27. <https://doi.org/10.1017/S0022112006009256>
- 562 Blaise, E., Suanez, S., Stéphan, P., Fichaut, B., David, L., Cuq, V., Autret, R., Houron, J.,  
563 Rouan, M., Floc'h, F., Ardhuin, F., Cancouët, R., Davidson, R., Costa, S., Delacourt, C.,  
564 2015. Bilan des tempêtes de l'hiver 2013-2014 sur la dynamique de recul du trait de côte en  
565 Bretagne. *Géomorphologie : relief, processus, environnement* 21, 267–292.  
566 <https://doi.org/10.4000/geomorphologie.11104>

- 567 Blondeaux, P., Vittori, G., 2011. The formation of tidal sand waves: Fully three-dimensional  
568 versus shallow water approaches. *Continental Shelf Research* 31, 990–996.  
569 <https://doi.org/10.1016/j.csr.2011.03.005>
- 570 Boudière, E., Maisondieu, C., Ardhuin, F., Accensi, M., Pineau-Guillou, L., Lepasqueur, J.,  
571 2013. A suitable metocean hindcast database for the design of Marine energy converters.  
572 *International Journal of Marine Energy* 3, e40–e52.  
573 <https://doi.org/10.1016/j.ijome.2013.11.010>
- 574 Charru, F., Andreotti, B., Claudin, P., 2013. Sand Ripples and Dunes. *Annual Review of Fluid*  
575 *Mechanics* 45, 469–493. <https://doi.org/10.1146/annurev-fluid-011212-140806>
- 576 Cruz, O.G., Noernberg, A.M., 2020. Bedforms controlled by residual current vortices in a  
577 subtropical estuarine tidal channel. *Estuarine, Coastal and Shelf Science* 232, 106485.  
578 <https://doi.org/10.1016/j.ecss.2019.106485>
- 579 Dalrymple, R.A., 1978. Rip currents and their causes. *Coastal Engineering 1978: Proceedings*  
580 *of the 16th International Conference. Am. Soc. Civ. Eng, New York*, pp.1414–1427.
- 581 Dalrymple, R.W., 1984. Morphology and internal structure of sandwaves in the Bay of Fundy.  
582 *Sedimentology* 31, 365–382. <https://doi.org/10.1111/j.1365-3091.1984.tb00865.x>
- 583 Doré, A., Bonneton, P., Marieu, V., Garlan, T., 2017. Observation and numerical modeling of  
584 tidal sand dune dynamics. *Coastal Dynamics* 90, 17–21
- 585 Ehrhold, A., Le Gall, B., Stéphan, P., Suanez, S.S., 2017. Présentation générale. In: Ehrhold,  
586 A., B.L.G. (Ed.), *Atlas de l'archipel de Molène. Géologie, Géomorphologie et*  
587 *Sédimentologie. Quae, Versailles*, pp. 17–32.
- 588 Elias, E.P.L., Hansen, J.E., 2013. Understanding processes controlling sediment transports at  
589 the mouth of a highly energetic inlet system (San Francisco Bay, CA). *Marine Geology* 345,  
590 207–220. <https://doi.org/10.1016/j.margeo.2012.07.003>
- 591 Ferret, Y., Bot, S.L., Tessier, B., Garlan, T., Lafite, R., 2010. Migration and internal architecture  
592 of marine dunes in the eastern English Channel over 14 and 56 year intervals: the influence  
593 of tides and decennial storms. *Earth Surface Processes and Landforms* 35, 1480–1493.  
594 <https://doi.org/10.1002/esp.2051>
- 595 Ferret, Y., Bot, S.L., Tessier, B., Garlan, T., Lafite, R., 2010. Migration and internal architecture  
596 of marine dunes in the eastern English Channel over 14 and 56 year intervals: the influence  
597 of tides and decennial storms. *Earth Surface Processes and Landforms* 35, 1480–1493.  
598 <https://doi.org/10.1002/esp.2051>



- 599 Flemming, B.W., 1978. Underwater sand dunes along the southeast African continental margin  
600 Observations and implications. *Marine Geology* 26, 177–198. [https://doi.org/10.1016/0025-](https://doi.org/10.1016/0025-3227(78)90059-2)  
601 [3227\(78\)90059-2](https://doi.org/10.1016/0025-3227(78)90059-2)
- 602 Fraccascia, S., Winter, C., Ernstsen, V.B., Hebbeln, D., 2016. Residual currents and bedform  
603 migration in a natural tidal inlet (Knudedyb, Danish Wadden Sea). *Geomorphology* 271, 74–  
604 83. <https://doi.org/10.1016/j.geomorph.2016.07.017>
- 605 Francken, F., Wartel, S., Parker, R., Taverniers, E., 2004. Factors influencing subaqueous dunes  
606 in the Scheldt Estuary. *Geo-Marine Letters* 24, 14–21. [https://doi.org/10.1007/s00367-003-](https://doi.org/10.1007/s00367-003-0154-x)  
607 [0154-x](https://doi.org/10.1007/s00367-003-0154-x)
- 608 Gregoire, G., 2016. Dynamique sédimentaire et évolution holocène d'un système macrotidal  
609 semi-fermé: l'exemple de la rade de Brest. Ph.D. Thesis. Université de Bretagne  
610 occidentale, Brest.
- 611 Gregoire, G., Ehrhold, A., Roy, P.L., Jouet, G., Garlan, T., 2016. Modern morpho-  
612 sedimentological patterns in a tide-dominated estuary system: the Bay of Brest (west  
613 Brittany, France). *Journal of Maps* 12, 1152–1159.  
614 <https://doi.org/10.1080/17445647.2016.1139514>
- 615 Gregoire, G., Le Roy, P., Ehrhold, A., Jouet, G., Garlan, T., 2017. Control factors of Holocene  
616 sedimentary infilling in a semi-closed tidal estuarine-like system: the bay of Brest (France).  
617 *Marine Geology* 385, 84–100. <https://doi.org/10.1016/j.margeo.2016.11.005>
- 618 Grochowski, N., Collins, M., Boxall, S., Salomon, J., Breton, M., Lafite, R., 1993. Sediment  
619 transport pathways in the eastern english-channel. *Oceanologica Acta* 16, 531–537.
- 620 Hallegouet, B., Lozac'h, G., Vigouroux, F., 1994. Formation de la rade de Brest. In : Corlaix,  
621 J.P. (Eds.), *Atlas permanent du littoral*. Editmar, France, p. 22.
- 622 Idier, D., Ehrhold, A., Garlan, T., 2002. Morphodynamique d'une dune sous-marine du détroit  
623 du pas de Calais. *Comptes Rendus Geoscience* 334, 1079–1085.
- 624 Knaapen, M. a. F., 2005. Sandwave migration predictor based on shape information. *Journal of*  
625 *Geophysical Research: Earth Surface* 110, F4. <https://doi.org/10.1029/2004JF000195>
- 626 Langhorne, D.N., 1973. A sandwave field in the Outer Thames Estuary, Great Britain. *Marine*  
627 *Geology* 14, 129–143. [https://doi.org/10.1016/0025-3227\(73\)90056-X](https://doi.org/10.1016/0025-3227(73)90056-X)
- 628 Le Bot, S., Trentesaux, A., Garlan, T., Berne, S., Chamley, H., 2000. Influence des tempêtes  
629 sur la mobilité des dunes tidales dans le détroit du Pas-de-Calais. *Oceanologica Acta* 23,  
630 129–141. [https://doi.org/10.1016/S0399-1784\(00\)00115-8](https://doi.org/10.1016/S0399-1784(00)00115-8)
- 631 Le Bot, S., Trentesaux, A., 2004. Types of internal structure and external morphology of  
632 submarine dunes under the influence of tide- and wind-driven processes (Dover Strait,

- 633 northern France). *Marine Geology* 211, 143–168.  
634 <https://doi.org/10.1016/j.margeo.2004.07.002>
- 635 Ma, X., Yan, J., Fan, F., 2014. Morphology of submarine barchans and sediment transport in  
636 barchans fields off the Dongfang coast in Beibu Gulf. *Geomorphology* 213, 213–224.  
637 <https://doi.org/10.1016/j.geomorph.2014.01.010>
- 638 Mallet, C., Howa, H.L., Garlan, T., Sottolichio, A., Hir, P.L., 2000. Residual Transport Model  
639 in Correlation with Sedimentary Dynamics over an Elongate Tidal Sandbar in the Gironde  
640 Estuary (Southwestern France). *Journal of Sedimentary Research* 70, 1005–1016.  
641 <https://doi.org/10.1306/022900701005>
- 642 McCave, I.N., 1971. Sand waves in the North sea off the coast of Holland. *Marine Geology* 10,  
643 199–225
- 644 Preston, J., Hurst, M.D., Mudd, S.M., Goodwin, G.C.H., Newton, A.J., Dugmore, A.J., 2018.  
645 Sediment accumulation in embayments controlled by bathymetric slope and wave energy:  
646 Implications for beach formation and persistence. *Earth Surface Processes and Landforms*  
647 43, 2421–2434. <https://doi.org/10.1002/esp.4405>
- 648 Reynaud, J.-Y., Dalrymple, R.W., 2012. Shallow-Marine Tidal Deposits, in: Davis, R.A.,  
649 Dalrymple, R.W. (Eds.), *Principles of Tidal Sedimentology*. Springer Netherlands,  
650 Dordrecht, pp. 335–369. [https://doi.org/10.1007/978-94-007-0123-6\\_13](https://doi.org/10.1007/978-94-007-0123-6_13)
- 651 Service Hydrographique et Océanographique de la Marine, SHOM. (1994). Atlas des courants  
652 de marée : Courants de marée de la côte Ouest de Bretagne. S.H.O.M, France.
- 653 Swift, D. J., 1976. Coastal sedimentation. In: Stanley, D.J. and Swift, D.J.P (Eds.), *Marine*  
654 *Sediment Transport and Environmental Management*, Wiley, New York, pp. 255-309.
- 655 Thauront, F., Berne, S. and Cirac, P., 1996. Tidal dune morphology and seasonal changes in  
656 the bay of Arcachon, France. *Comptes Rendus de l'Académie des Sciences de Paris (II a)*,  
657 323, pp. 411-418.
- 658 Todd, B.J., 2005. Morphology and composition of submarine barchan dunes on the Scotian  
659 Shelf, Canadian Atlantic margin. *Geomorphology* 67, 487–500.  
660 <https://doi.org/10.1016/j.geomorph.2004.11.016>
- 661 Van Dijk, T.A.G.P., Kleinhans, M.G., 2005. Processes controlling the dynamics of compound  
662 sand waves in the North Sea, Netherlands. *Journal of Geophysical Research: Earth Surface*  
663 110, Issue F4. <https://doi.org/10.1029/2004JF000173>

- 664 Van Landeghem, K.J.J., Wheeler, A.J., Mitchell, N.C., Sutton, G., 2009. Variations in sediment  
665 wave dimensions across the tidally dominated Irish Sea, NW Europe. *Marine Geology* 263,  
666 108–119. <https://doi.org/10.1016/j.margeo.2009.04.003>
- 667 Van Landeghem, K.J.J., Baas, J.H., Mitchell, N.C., Wilcockson, D., Wheeler, A.J., 2012.  
668 Reversed sediment wave migration in the Irish Sea, NW Europe: A reappraisal of the validity  
669 of geometry-based predictive modelling and assumptions. *Marine Geology* 295, 95–112.  
670 <https://doi.org/10.1016/j.margeo.2011.12.004>
- 671 Van Santen, R.B., de Swart, H.E., van Dijk, T.A.G.P., 2011. Sensitivity of tidal sand  
672 wavelength to environmental parameters: A combined data analysis and modelling  
673 approach. *Continental Shelf Research* 31, 966–978.  
674 <https://doi.org/10.1016/j.csr.2011.03.003>
- 675 Yalin, M.S., 1964. Geometrical Properties of Sand Wave. *Journal of the Hydraulics Division*  
676 90, 105–119.  
677  
678

### **Highlights**

- 1) Channelised tidal currents in macrotidal environment induce large variation in dune migration rates across a dune field at the outlet of the Bay of Brest.
- 2) Hydrodynamic forcing by tidal currents combining bi-directional currents in the channel and a tidal gyre in the shallower nearshore terrace allow the recirculation of sediment from dune field through external pathways.
- 3) The location of the dune field *extending on the channel floor and along the steep side of the channel* shows the impact of varying bottom slopes on dune migration rates, with reduced rates on the negative slopes and increased rates on the positive slopes.

**Declaration of interests**

The authors declare that they have no known competing financial interests or personal relationships that could have appeared to influence the work reported in this paper.

The authors declare the following financial interests/personal relationships which may be considered as potential competing interests:

Journal Pre-proof